Available online at www.sciencedirect.com

SciVerse ScienceDirect

Procedia IUTAM 00 (2012) 000-000

Procedia IUTAM

www.elsevier.com/locate/procedia

Topological Fluid Dynamics II

Motion of axisymmetric magnetic eddies with swirl

Yuji Hattori[a], Stefan G. Llewellyn Smith[b]

[a]*Institute of Fluid Science, Tohoku University, Sendai 980–8577, Japan*
[b]*Department of Mechanical and Aerospace Engineering, Jacobs School of Engineering, UCSD, 9500 Gilman Drive, La Jolla CA 92093-0411, USA*

Abstract

We consider the motion of axisymmetric magnetic eddies with swirl in ideal magnetohydrodynamic (MHD) flow. The magnetic field is assumed to be toroidal, while the velocity field has both toroidal and poloidal components. The contour-dynamics formulation by Hattori and Moffatt (2006) for the case without swirl is extended to include swirl velocity so that the cross helicity does not vanish in general. The strength of the vortex sheets that appear on the contours varies with time under the influence of the centrifugal force due to swirl and the magnetic tension due to the Lorentz force. Numerical simulation using the contour-dynamics formulation shows that there exist counter-propagating dipolar structures whose radius is given by a balance between the centrifugal force and the magnetic tension. These structures are well described by the steady solutions obtained by perturbation expansion. The effects of vorticity inside the eddy on the motion of eddies are also investigated.

Keywords: magnetohydrodynamics (MHD); cross helicity; contour dynamics

1. Introduction

The motion of magnetic eddies, which are compact vortices with magnetic field, is of much interest in astrophysical fluid dynamics and plasma physics for which magnetohydrodynamics (MHD) is often a good approximation to the full equations of motion. Although steady structures and coherent structures are frequently encountered in MHD, our knowledge of these structures is far from sufficient since nonlinearity of the dynamics makes it difficult to find exact solutions of the equations of motion. It is hence helpful to find new exact solutions which describe magnetic eddies. To this end Hattori and Moffatt [1] (hereafter referred to as HM06) have found a family of exact solutions which include Hill's spherical vortex as a limiting case. They also found a contour dynamics formulation of ideal axisymmetric MHD. Using contour dynamics quasi-steady structures which are well approximated by the exact solutions were found to form by numerical simulation.

In the context of topological fluid dynamics the roles of magnetic helicity and cross helicity, both of which have topological interpretation and are conserved in MHD, are of interest. One of the significant roles is that both helicities

* Corresponding author. Tel.: +81-22-217-5256 ; fax: +81-22-217-5256 .
E-mail address: hattori@fmail.ifs.tohoku.ac.jp

give bounds for hydrodynamic and magnetic energy. The magnetic helicity $H_M = \int \boldsymbol{A}\cdot\boldsymbol{B}\,\mathrm{d}V$ gives a bound proportional to $|H_M|$ [2, 3]. HM06 considered the case $H_M = 0$ so that this bound is zero. It was expected that magnetic energy decreases to zero since magnetic tension due to the Lorentz force is directed toward the axis of symmetry so that the eddy collapses to the axis. Magnetic energy, however, could not decrease to zero because the quasi-steady structures kept a finite amount of magnetic energy. On the other hand the cross helicity $H_C = \int \boldsymbol{u}\cdot\boldsymbol{B}\,\mathrm{d}V$ gives

$$\frac{E_T}{2} - \frac{1}{2}\left(E_T^2 - H_C^2\right)^{1/2} \le E_X \le \frac{E_T}{2} + \frac{1}{2}\left(E_T^2 - H_C^2\right)^{1/2}, \tag{1}$$

where $X = H, M$ $E_H = \frac{1}{2}\int |\boldsymbol{u}|^2\,\mathrm{d}V$ is the hydrodynamic energy, $E_M = \frac{1}{2}\int |\boldsymbol{B}|^2\,\mathrm{d}V$ is the magnetic energy and $E_T = E_H + E_M$. Since the total energy E_T is also conserved, the motion of the eddy is constrained by the above inequality whose bounds are determined by initial conditions. The cross helicity is also zero in HM06 implying that this inequality is trivial.

Recently we have extended the above work to the magnetic eddies with swirl [4]. We have found a family of exact solutions which include classical vortex rings with swirl [5]. Exact solutions of spherical shape were classified. The contour dynamics formulation was also extended to include swirl or toroidal component of velocity. The unsteady evolution simulated by contour dynamics in the case including both swirl and magnetic field was shown to lead to a splitting of the initial configuration and the appearance of two counter-propagating vortex dipoles.

In this paper we study the motion of magnetic eddies with swirl. We are particularly interested in two problems. One is how the bounds determined by cross helicity constrain the motion of the eddies. Since cross helicity does not vanish for eddies with swirl, the inequality (1) limits the range of hydrodynamic and magnetic energy. The other is the effects of vorticity inside the eddies. In the previous contour dynamics simulations [1, 4] the vorticity of finite magnitude inside the eddy is set to zero. In this study we consider the case with non-vanishing vorticity inside the eddy and see how it affects the motion.

2. Contour Dynamics

We recall the contour dynamics formulation of the motion of magnetic eddies with swirl [4]. We consider an axisymmetric ideal MHD flow whose magnetic field has only a toroidal component B_θ, while the velocity field has all three components in general. Then the toroidal components of velocity field u_θ, the vorticity ω_θ and the magnetic field B_θ are governed by

$$\frac{\mathrm{D}}{\mathrm{D}t}\left(\frac{\omega_\theta}{r}\right) = \frac{1}{r^2}\frac{\partial}{\partial z}\left(u_\theta^2 - B_\theta^2\right), \quad \frac{\mathrm{D}}{\mathrm{D}t}\left(ru_\theta\right) = 0, \quad \frac{\mathrm{D}}{\mathrm{D}t}\left(\frac{B_\theta}{r}\right) = 0. \tag{2}$$

The above equations lead us to consider the following type of distribution

$$\frac{\omega_\theta}{r} = \Gamma(r,z,t)\delta\left[f(r,z,t)\right]|\nabla f| + \Omega_c H\left[f(r,z,t)\right], \quad u_\theta = \frac{C}{r}H\left[f(r,z,t)\right], \quad B_\theta = \kappa r H\left[f(r,z,t)\right],$$

where Γ is the θ-component of the strength of the vortex sheet, C, κ and Ω_c are constants and $H[\cdot]$ is the Heaviside function; ω_θ, u_θ and B_θ are non-zero only inside a closed region D in rz-plane defined by $f(r,z,t) > 0$. Then the motion of the eddy can be specified by the contour $f(r,z,t) = 0$ and the strength of vortex sheet on it. Let us parametrize the contour as $(r,z) = (R(s,t), Z(s,t))$ where s is the parameter along the contour. Introducing $\gamma = \Gamma R\left[\left(\frac{\partial R}{\partial s}\right)^2 + \left(\frac{\partial Z}{\partial s}\right)^2\right]^{1/2}$, we obtain the following set of equations which completely determines the motion of the

contour [4, 6]

$$\frac{\partial \gamma}{\partial t} = \left(\kappa^2 R - \frac{C^2}{R^3}\right)\frac{\partial R}{\partial s}, \tag{3}$$

$$\frac{\partial R}{\partial t} = u_r(R(s,t),Z(s,t),t) + u_{\omega,r}(R(s,t),Z(s,t),t), \quad \frac{\partial Z}{\partial t} = u_z(R(s,t),Z(s,t),t) + u_{\omega,z}(R(s,t),Z(s,t),t), \tag{4}$$

$$u_r = \frac{1}{r}\oint \gamma(s,t)\left[\frac{\partial}{\partial z}G(r,z|R(s,t),Z(s,t))\right]\,\mathrm{d}s, \quad u_z = -\frac{1}{r}\oint \gamma(s,t)\left[\frac{\partial}{\partial r}G(r,z|R(s,t),Z(s,t))\right]\,\mathrm{d}s. \tag{5}$$

$$u_{\omega,r} = -\Omega_c \oint QR(s,t)\frac{\partial R(s,t)}{\partial s}\,\mathrm{d}s, \quad u_{\omega,z} = -\Omega_c \oint \left[P(Z(s,t)-z)\frac{\partial R(s,t)}{\partial s} + Qr\frac{\partial Z(s,t)}{\partial s}\right]\,\mathrm{d}s, \tag{6}$$

where

$$G(r,z|r',z') = \frac{1}{2\pi}(rr')^{1/2}\left[\left(\frac{2}{k}-k\right)K(k) - \frac{2}{k}E(k)\right], \quad k^2 = \frac{4rr'}{(r+r')^2+(z-z')^2}, \tag{7}$$

$$P(r,z|r',z') = \frac{r'K(k)}{\pi\left[(r+r')^2+(z-z')^2\right]^{1/2}}, \tag{8}$$

$$Q(r,z|r',z') = \frac{1}{2\pi r}\left[\frac{r^2+r'^2+(z-z')^2}{\left[(r+r')^2+(z-z')^2\right]^{1/2}}K(k) - \left[(r+r')^2+(z-z')^2\right]^{1/2}E(k)\right]. \tag{9}$$

Here K and E are the complete integrals of the first and second kind, respectively.

There are several constants of motion under the above equations, including the total energy E_T, the cross helicity H_C and the volume V. In the present formulation cross helicity is related to volume by $H_C = \kappa CV$.

The contour dynamics formulation enables us to numerically simulate the axisymmetric MHD flow by one-dimensional discretization in space; we just need to follow the time evolution of a closed curve and a function on it. This simplification reduces time for numerical simulation. Moreover it is easy to generalize the above formulation to multiple contours to approximate continuous distributions of u_θ and B_θ [4].

3. Numerical Results

3.1. Numerical Methods

The numerical method is similar to that used in HM06. The contour is expressed by a set of discrete points. The integrands of (5) and (6) have singularities at $r = r'$. We subtract the contribution by the singular parts whose principal values are known, calculate the resulting regular parts numerically and add them to obtain numerical values of (5) and (6). Furthermore as in HM06 we regularize the integrands in (5) to avoid the vortex sheet singularity [7, 8], while regularization is not required for $\boldsymbol{u}_\omega$. Remeshing is applied in order to prevent the distance between the points from becoming too small or too large.

In order to check the added part $\boldsymbol{u}_\omega$ we calculated the steady motion of a vortex ring by setting $C = \kappa = 0$ and $\Omega_c = 1$. The speed of the translational motion was in good agreement with the theoretical value [9].

3.2. Motion of eddy and bounds for energy

Here we study time evolution of hydrodynamic and magnetic energies to see how they behave within the bounds given by cross helicity. We set $\kappa = C = 1$ and $\Omega_c = 0$. We consider magnetic eddies of a torus type. Initially the contour in rz-plane is set to be a circle of radius 0.2 with no poloidal component of velocity: $\gamma = 0$. Three different values are chosen for the initial center of the circle or radius of the eddy: $R_0 = 0.8, 1.0$ and 1.2.

The motion of the eddy is drived by two forces: the Lorentz force which is directed toward the axis of symmetry and the centrifugal force directs radially outward. There is an equilibrium radius at which the Lorentz and centrifugal

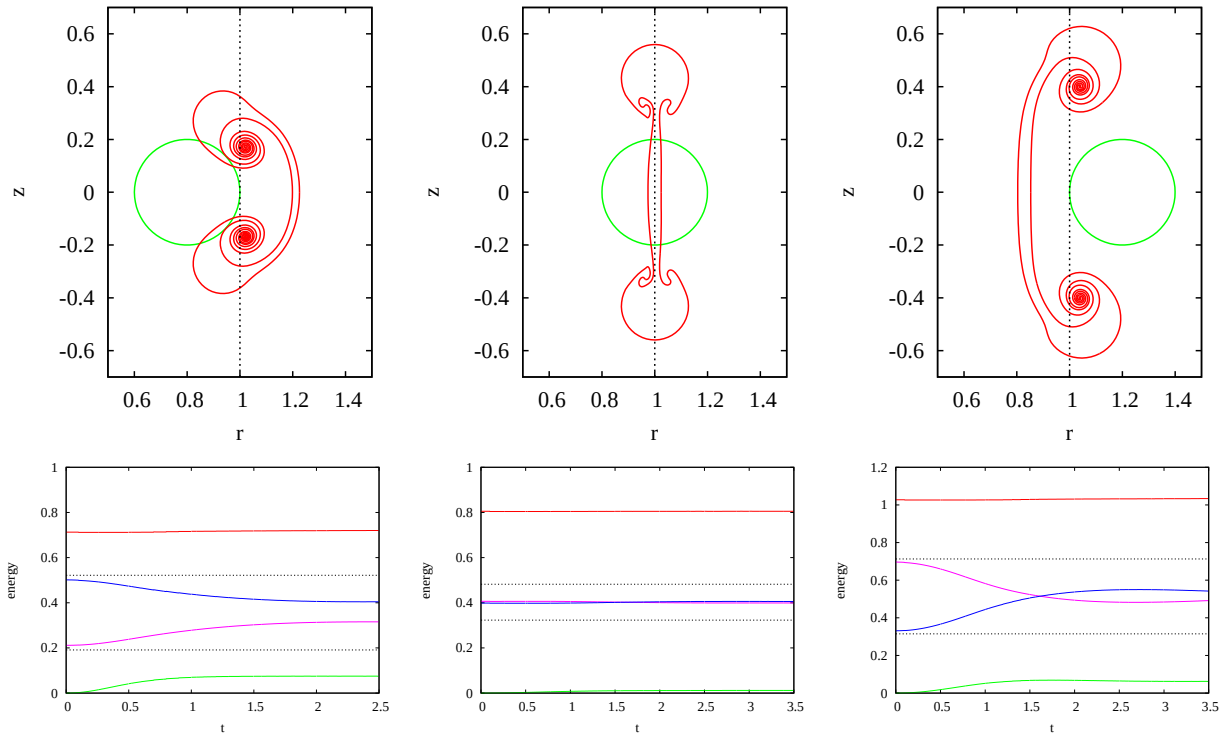

Fig. 1. Time evolution of eddy and energies. Top: contours at the initial (green) and final (red) instants; the dotted lines show the equilibrium radius $r = R_b$. Bottom: time evolution of total energy E_T (red), hydrodynamic energy E_H (blue), magnetic energy E_M (purple) and poloidal component of hydrodynamic energy E_{HT}; the dotted lines show the bounds for E_H and E_M in (1). Left: $R_0 = 0.8$, center: $R_0 = 1$, right: $R_0 = 1.2$.

forces balance given by

$$R_b = \left(\frac{C}{\kappa}\right)^{1/2}. \tag{10}$$

In $r < R_b$ and $r > R_b$ the outward centrifugal force is larger and smaller than the inward Lorentz force, respectively. As a result the net force acts as a restoring force that drives the eddy towards the equilibrium radius $r = R_b$.

Figure 1 shows the time evolution of energy, along with the contour at the initial and final instants of simulation for the three values of the initial radius of the eddy. In the top figures the initial and final contours are shown by the green and red lines, respectively. For $R_0 = 1.0$ the eddy splits into two rings which propagate in opposite direction along $r = R_b$. For $R_b = 0.8$ the eddy not only splits but also moves to the equilibrium radius, while a thin thread connecting the two rings crosses the equilibrium radius. The roll up observed behind the two rings is due to the regularization of the integrand. The two split rings move along $r = R_b$ like those for $R_0 = 1.0$. The same behavior, with reversed direction, is observed for $R_0 = 1.2$.

In the bottom panels of Fig. 1, t the time evolution of total energy E_T, hydrodynamic energy E_H, magnetic energy E_M and poloidal component of hydrodynamic energy $E_{HP} = \frac{1}{2}\int (u_r^2 + u_z^2)\, \mathrm{d}V$ are shown by the red, blue, purple and green lines, respectively. The dotted lines show the bounds for E_H and E_M in (1); E_H and E_M should be between the bounds, while E_{HP} need not. For $R_0 = 1.0$ all energies are almost unchanged. For $R_0 = 0.8$ and 1.2 the initial values of E_H and E_M are close to the bounds. The values approach $E_T/2$ as time proceeds. This is consistent with the motion since the toroidal component of the hydrodynamic energy $E_{HT} = \frac{1}{2}\int u_\theta^2\, \mathrm{d}V$ is close to E_M near $r = R_b$. At large t the poloidal component of the hydrodynamic energy E_{HP} is responsible for the difference between E_H and E_M.

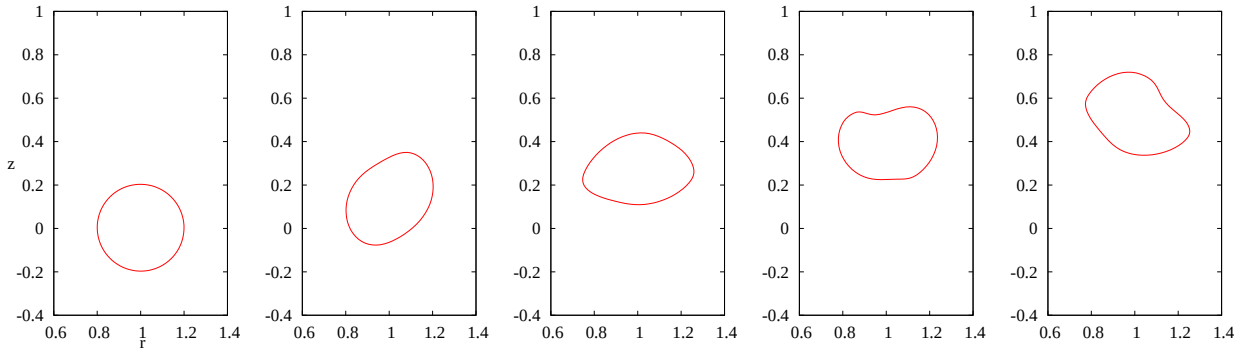

Fig. 2. Motion of magnetic eddies. $\kappa = C = 0.2, \Omega_c = 1$. From left to right: $t = 0, 4, 8, 12$ and 16.

3.3. *Effects of vorticity inside the eddy*

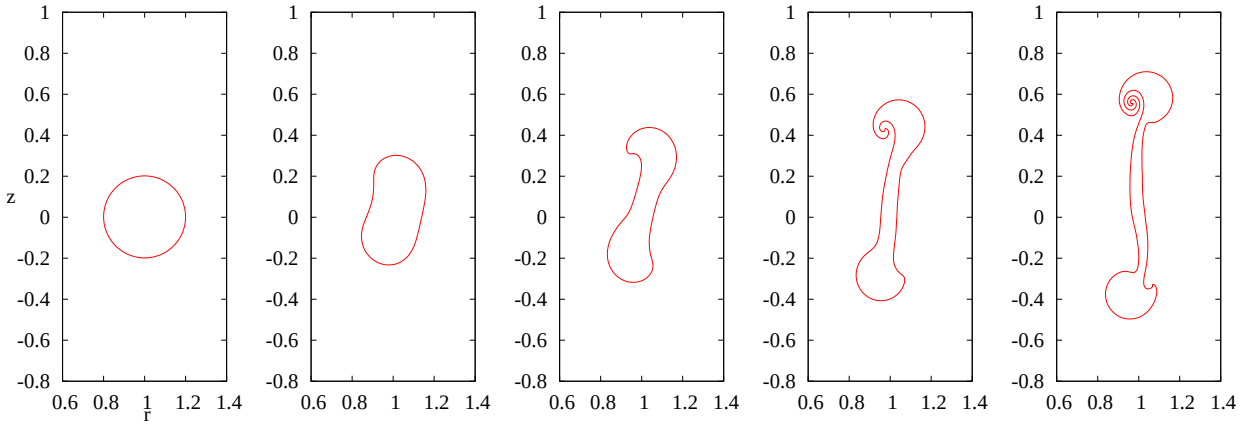

Fig. 3. Motion of magnetic eddies. $\kappa = C = 1, \Omega_c = 1$. From left to right: $t = 0, 1, 2, 3$ and 4.

Next we investigate the effects of vorticity inside the eddy setting a non-zero value for Ω_c. We fix $\Omega_c = 1$ and use two values of $\kappa = C = 0.2$ and 1.0. As in the previous section γ is set to zero initially. The initial radius R_0 is set to $R_0 = R_b = 1$.

Figure 2 shows the motion of the eddy for $\kappa = C = 0.2$. The eddy propagates with constant speed in $+z$ direction. The contour deforms into an elliptical shape with its axis rotating around the center of the contour. The motion is similar to that of a vortex ring which corresponds to $\kappa = C = 0$, while the deformation is larger than a vortex ring. When there is non-vanishing vorticity inside the eddy and $\kappa = C$ is small, the vortex sheet on the contour cannot acquire large strength not only because the forces are weak and but also because the contour is rotating so that the rate of change of γ changes its sign.

Figure 3 shows the motion of the eddy for $\kappa = C = 1.0$. In this case the motion is similar with the case $\Omega_c = 0$ [4]; the initial single eddy splits into two counter-propagating rings. However, the contour is asymmetric with respect to $z = 0$. The mid-point of the two rings moves slowly in $+z$-direction owing to the self-induced velocity by vorticity inside the eddy. In addition the radial positions of the centers of the upper and lower rings are larger and smaller respectively than the equilibrium radius $r = R_b$. This is explained by the steady solution described in the next section.

4. Steady solutions

Steady solutions in the presence of uniform vorticity inside the eddy can be found by a perturbation expansion assuming the ratio of core to ring radius of the eddy ε be small. We introduce $(\tilde{r},\tilde{z}) = ((r-R_0)/(\varepsilon R_0), z/(\varepsilon R_0))$, where R_0 is the ring radius of the eddy. As in the preceding sections we assume

$$u_\theta = \frac{C}{R_0\,(1+\varepsilon\tilde{r})}, \quad B_\theta = \kappa R_0(1+\varepsilon\tilde{r}), \tag{11}$$

inside the core, and $u_\theta = B_\theta = 0$ outside. Then the steady MHD equations become

$$u_r\frac{\partial u_r}{\partial\tilde{r}} + u_z\frac{\partial u_r}{\partial\tilde{z}} + \frac{\partial p_*}{\partial\tilde{r}} = \varepsilon\left(\frac{u_\theta^2}{1+\varepsilon\tilde{r}} - \frac{B_\theta^2}{1+\varepsilon\tilde{r}}\right), \tag{12}$$

$$u_r\frac{\partial u_z}{\partial\tilde{r}} + u_z\frac{\partial u_z}{\partial\tilde{z}} + \frac{\partial p_*}{\partial\tilde{z}} = 0, \tag{13}$$

$$\frac{\partial u_r}{\partial\tilde{r}} + \frac{\partial u_z}{\partial\tilde{z}} = -\varepsilon\frac{u_r}{1+\varepsilon\tilde{r}}. \tag{14}$$

The other variables are expanded as

$$u_r = u_r^{(0)} + \varepsilon u_r^{(1)} + \cdots, \quad u_z = u_z^{(0)} + \varepsilon u_z^{(1)} + \cdots, \quad p_* = p_*^{(0)} + \varepsilon p_*^{(1)} + \cdots. \tag{15}$$

We fix κ and R_0, while C is expanded as $C = C_0 + \varepsilon C_1 + \cdots$ since in general R_0 does not coincide with the equilibrium radius R_b.

At the leading order the equations coincides with those for two-dimensional steady inviscid hydrodynamic flow with pressure being replaced by the total pressure. We choose a trivial leading-order solution $u_r^{(0)} = u_z^{(0)} = 0$, $p_*^{(0)} =$ const. At the next order the equations are

$$\frac{\partial p_*^{(1)}}{\partial\tilde{r}} = \left(\frac{C_0^2}{R_0^2} - \kappa^2 R_0^2\right) H[1-\tilde{r}^2-\tilde{z}^2], \quad \frac{\partial p_*^{(1)}}{\partial\tilde{z}} = 0, \quad \frac{\partial u_r^{(1)}}{\partial r} + \frac{\partial u_z^{(1)}}{\partial z} = 0, \tag{16}$$

from which we obtain

$$C_0 = \kappa R_0^2, \quad p_*^{(1)} = 0. \tag{17}$$

At $O(\varepsilon^2)$ the equations are

$$u_r^{(1)}\frac{\partial u_r^{(1)}}{\partial\tilde{r}} + u_z^{(1)}\frac{\partial u_r^{(1)}}{\partial\tilde{z}} + \frac{\partial p_*^{(2)}}{\partial\tilde{r}} = -4\kappa^2 R_0^2 H[1-\tilde{r}^2-\tilde{z}^2]\tilde{r} + 2\kappa C_1 H[1-\tilde{r}^2-\tilde{z}^2], \tag{18}$$

$$u_r^{(1)}\frac{\partial u_z^{(1)}}{\partial\tilde{r}} + u_z^{(1)}\frac{\partial u_z^{(1)}}{\partial\tilde{z}} + \frac{\partial p_*^{(2)}}{\partial\tilde{z}} = 0, \quad \frac{\partial u_r^{(2)}}{\partial\tilde{r}} + \frac{\partial u_z^{(2)}}{\partial\tilde{z}} = 0. \tag{19}$$

We seek a solution which describes the structures observed in the preceding sections. We set

$$u_r^{(1)} = \frac{\Omega_c}{2}\tilde{z}, \quad u_z^{(1)} = -\frac{\Omega_c}{2}\tilde{r}, \tag{20}$$

inside the eddy $\tilde{r}^2+\tilde{z}^2 < 1$. Then

$$p_*^{(2)} = p_{*,02} - 2\kappa^2 R_0^2\tilde{r}^2 + \frac{\Omega^2}{8}(\tilde{r}^2+\tilde{z}^2) + 2\kappa C_1\tilde{r}. \tag{21}$$

Outside the eddy $r^2+z^2 > 1$ the solution is

$$u_r^{(1)} = \kappa R_0\frac{2\tilde{r}\tilde{z}}{(\tilde{r}^2+\tilde{z}^2)^2} - \beta\frac{\tilde{z}}{\tilde{r}^2+\tilde{z}^2}, \quad u_z^{(1)} = -\kappa R_0\left(1+\frac{\tilde{r}^2-\tilde{z}^2}{(\tilde{r}^2+\tilde{z}^2)^2}\right) + \beta\frac{\tilde{r}}{\tilde{r}^2+\tilde{z}^2},$$

$$p_*^{(2)} = -\kappa^2 R_0^2\frac{\tilde{r}^2-\tilde{z}^2+\frac{1}{2}}{(\tilde{r}^2+\tilde{z}^2)^2} + \beta\kappa R_0\tilde{r}\left(\frac{1}{\tilde{r}^2+\tilde{z}^2} + \frac{1}{(\tilde{r}^2+\tilde{z}^2)^2}\right) - \frac{\beta^2}{2(\tilde{r}^2+\tilde{z}^2)}$$

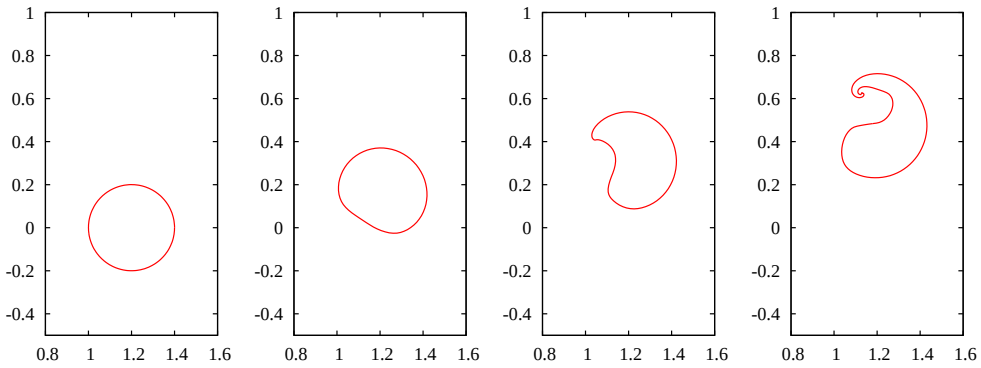

Fig. 4. Motion of magnetic eddies. Steady solution. $\kappa = C = 0.25, \Omega_c = 1$. From left to right: $t = 0, 2, 4$ and 6.

Since the pressure should be continuous we have $C_1 = \beta$. The θ-component of the strength of the vortex sheet is

$$\Omega^{(1)} = -2\kappa R_0 \cos\varphi + \frac{\Omega_c}{2} + \beta, \tag{22}$$

where $\varphi = \tan^{-1}(\tilde{z}/\tilde{r})$. If the total circulation is zero then $\Omega/2 + \beta = 0$ and the center of the cross section differs from the equilibrium radius by

$$\Delta R = R_b - R_0 = \frac{\varepsilon\beta}{2\kappa} = -\frac{\varepsilon\Omega_c}{4\kappa}. \tag{23}$$

Up to this order the outer solution is the same as the potential flow around a rotating cylinder. The deviation from the equilibrium radius ΔR is due to the Magnus force. At higher order the boundary should deform.

The steady solutions obtained above are verified by numerical simulation (Fig. 4). As in HM06 a part of the contour or core boundary moves without deformation at the predicted velocity. An instability is also observed initially at the rear side ($t = 2$), while the unstable part rotates clockwise with large deformation ($t = 4$ and 6).

5. Concluding Remarks

The motion of magnetic eddies with interior vorticity in the presence of swirl is studied by contour dynamics simulation. First, the bounds for hydrodynamic and magnetic energy determined by cross helicity are checked by numerical simulation. Starting from the values close to the bounds, both energies become close to a half of the total energy as the eddy approaches the equilibrium radius where the Lorentz and centrifugal forces balance.

Next, the effects of vorticity inside the eddy are investigated. Depending on the magnitude of the Lorentz and centrifugal forces two types of motion are observed. For small forces the motion of the eddy is similar to that of a vortex ring; it propagates with constant speed with its boundary or contour oscillating. For large forces the eddy splits into two counter-propagating rings. A steady solution which describes these rings is obtained by perturbation expansion assuming the ratio of core to ring radius be small. Future works would include finding steady solutions generally without this assumption, using theoretical or numerical methods.

Acknowledgements

This research was supported by Collaborative Research Project 2010 and 2011, Institute of Fluid Science, Tohoku University, Project Code J10022 and J11029.

References

[1] Hattori Y, Moffatt YK. Evolution of toroidal magnetic eddies in an ideal fluid. *J. Fluid Mech.* 2006;558:253–279.

[2] Arnold, V. I. The asymptotic Hopf invariant and its application. In: *Differential Equations*. Erevan. Armenian SSR Acad. Sci. (in Russian) (English transl. *Sel. Math. Sov.* 1985;5:327–345.)

[3] Moffatt YK. Magnetostatic equilibria and analogous Euler flows with arbitrary complex topology Part 1. Fundamentals. *J. Fluid Mech.* 1986;159:359–378.

[4] Llewellyn Smith SG, Hattori Y. Axisymmetric magnetic vortices with swirl. *Comm. Nonlinear Sci. Numer. Simulat.* 2012;17:2101–2107.

[5] Hicks WM. Researches in vortex motion. Part III: On spiral or gyrostatic vortex aggregates. *Philos. T. Roy. Soc.* A 1899;192:33–99.

[6] Wakelin SL, Riley N. Vortex ring interactions II. inviscid models. *Q. J. Mech. Appl. Math.* 1996;49:287–309.

[7] Krasny R. A study of singularity formation in a vortex sheet by the point-vortex approximation. *J. Fluid Mech.* 1986;167:65–93.

[8] Krasny R. Computation of vortex sheet roll-up in the Trefftz plane. *J. Fluid Mech.* 1987;184:123–155.

[9] Saffman PG. *Vortex Dynamics*. Cambridge Univ. Press; 1992.